A Simulation Study of Spectral Čerenkov Luminescence Imaging for Tumour Margin Estimation

Nick Calvert[d], Yusef Helo[b], Thomy Mertzanidou[b], David S. Tuch[a], Simon R. Arridge[b,c], and Danail Stoyanov[b,c]

[a]Lightpoint Medical Ltd, The Island, Moor Road, Chesham, HP5 1NZ, United Kingdom
[b]Centre for Medical Image Computing, University College London, Gower Street, WC1E 6BT, United Kingdom
[c]Department of Computer Science, University College London, Gower Street, WC1E 6BT, United Kingdom
[d]Department of Medical Physics and Biomedical Engineering, University College London, Gower Street, WC1E 6BT, United Kingdom

ABSTRACT

Breast cancer is the most common cancer in women in the world. Breast-conserving surgery (BCS) is a standard surgical treatment for breast cancer with the key objective of removing breast tissue, maintaining a negative surgical margin and providing a good cosmetic outcome. A positive surgical margin, meaning the presence of cancerous tissues on the surface of the breast specimen after surgery, is associated with local recurrence after therapy. In this study, we investigate a new imaging modality based on Čerenkov luminescence imaging (CLI) for the purpose of detecting positive surgical margins during BCS. We develop Monte Carlo (MC) simulations using the Geant4 nuclear physics simulation toolbox to study the spectrum of photons emitted given ^{18}F-FDG and breast tissue properties. The resulting simulation spectra show that the CLI signal contains information that may be used to estimate whether the cancerous cells are at a depth of less than 1 mm or greater than 1 mm given appropriate imaging system design and sensitivity. The simulation spectra also show that when the source is located within 1 mm of the surface, the tissue parameters are not relevant to the model as the spectra do not vary significantly. At larger depths, however, the spectral information varies significantly with breast optical parameters, having implications for further studies and system design. While promising, further studies are needed to quantify the CLI response to more accurately incorporate tissue specific parameters and patient specific anatomical details.

Keywords: Čerenkov Imaging, BCS, surgical margin imaging

1. INTRODUCTION

Breast cancer is the most common cancer in women in the world. Breast-conserving surgery (BCS) is a standard surgical treatment for breast cancer with the key objective of removing breast tissue, maintaining a negative surgical margin and providing a good cosmetic outcome.[1] A positive surgical margin, meaning the presence of cancerous tissues on the surface of the breast specimen after surgery, is associated with local recurrence after therapy, although estimates of effects vary between studies (see e.g.[2]). Negative margins cannot always be reliably assessed intraoperatively, and cases with positive margins, which occur in $15-40\%$ of procedures,[3] and detected at pathology and require a further surgery. As a consequence, there is an unmet need to assess surgical margin status in real time during surgery to ensure that all of the cancer is completely removed. A technology which can accurately identify cancer cells at the surgical margin would improve surgical precision and could lead to a significant improvement in patient and healthcare outcomes.

Further author information: (Send correspondence to D.S.)
D.S.: E-mail: danail.stoyanov@ucl.ac.uk.
N.C. is now at Rapiscan Systems Ltd, Bonehurst Road, RH1 5GG, United Kingdom.

Medical Imaging 2017: Biomedical Applications in Molecular, Structural, and Functional Imaging
edited by Andrzej Krol, Barjor Gimi, Proc. of SPIE Vol. 10137, 1013717 · © 2017 SPIE
CCC code: 1605-7422/17/$18 · doi: 10.1117/12.2254407

Current standard of care is the post-surgical assessment of tumour margins by a histopathologist examining a haematoxylin and eosin stained frozen section.[4,5] The results are obtained too late to impact surgical decision making and intra-operative imaging of Čerenkov emissions from radioisotopes concentrated in cancer cells could have a significant transformative impact. Visualisation of emitted light from cancer during surgery would enable the surgeon to assess surgical margin status during the procedure and remove additional tissue as necessary. This can be performed by using specimen analyser imaging systems such as the LightPath$^{\text{TM}}$ developed by Lightpoint Medical. This device relies on detecting the photons emitted by radiotracer administration which congregates within the cancerous tissue. While early results of the capabilities of such a system have been shown,[6] the depth of the emission is still unknown. In this study, we investigate whether it is theoretically possible to estimate this depth by using Monte Carlo (MC) simulations. The purpose of the investigation is to identify specific spectral bands which may be interrogated to solve for depth localisation which would allow effective surgical margin assessment at the surface of an image sample.

2. CERENKOV LUMINESCENSE IMAGING

Čerenkov luminescence imaging (CLI) is a molecular imaging technique based on the detection of Čerenkov photons induced by β^+ particles emitted by a radioactive tracer. When β^+ particles travel through tissue with a velocity greater than the phase velocity of light in the tissue, asymmetrical local polarisation of the tissue molecules along the particle path occurs. When these polarised molecules relax to their ground state, energy is lost in the form of visible light.[7,8]

The velocity of a β^+ particle with energy E keV is

$$v = c\left(1 - \frac{E_0^2}{(E+E_0)^2}\right)^{1/2}, \tag{1}$$

where c is the speed of light in a vacuum, and E_0 is the rest-mass energy of a β^+ particle (511 keV). The number of Čerenkov photons generated over the path of a particle, in the spectral range (λ_1, λ_2) is given by the Frank-Tamm formula[9,10]

$$\frac{\partial N}{\partial x} = 2\pi\alpha\left(\frac{1}{\lambda_1} - \frac{1}{\lambda_2}\right)\int_{\lambda_1}^{\lambda_2}\frac{1}{\lambda^2}\,d\lambda \quad \text{for } \phi n > 1, \tag{2}$$

$$\frac{\partial N}{\partial x} = 0 \quad \text{for } \phi n \leq 1, \tag{3}$$

where $\alpha = 1/137$ is the fine structure constant, n is the refractive index of the material, and $\phi = v/c$. For tissue with a refractive index of 1.4, the Čerenkov production threshold ($\phi n > 1$) is 219.2 keV, and the yield increases with increasing β^+ energy.

CLI is a rapidly emerging techniques that bridges optical (typically preclinical) imaging and nuclear (clinical) imaging using clinically-available PET radiopharmaceuticals. In breast cancer, the PET radiopharmaceutical 18F-FDG is most-commonly used. The positrons emitted by the source generate Čerenkov photons in the tissue. The Čerenkov photons are detected using a highly sensitive optical camera, such as a charge-coupled device (CCD). The ^{18}F-FDG accumulates at regions of upregulated metabolism, e.g. malignant tumours. This leads to high Čerenkov counts from these tumours, when compared to the background.

A full review of CLI is outside the scope of this work, see e.g.,[7,10,11] however, one particular area of interest is the interrogation of spectral bands to estimate tumour depth. The number of Čerenkov photons reaching a detector is dependent upon the absorption and scattering coefficients of the tissue, which are non-uniform across the spectral range of the emitted photons. By measuring two spectral bands separately, e.g. by placing a low-pass filter in front of one camera and a high-pass filter in front of another, and comparing the detected counts, a depth estimation model can be generated. This model is based on MC simulations of Čerenkov photons at different depths in tissue. This work is novel because we explore how different tissue parameters affect the recorded Čerenkov spectrum and we attempt to estimate the depth of the Čerenkov photons based on the recorded spectrum.

3. MODEL DESCRIPTION

A MC model was written using the Geant4 toolbox,[12] simulating the transport of the positrons and Čerenkov photons through the medium. The geometry consisted of a $10 \times 10 \times 10$ mm cube of glandular tissue, representing a section of breast tissue. The positron source was a 2 mm radius cylinder, 0.1 mm in length, placed in the middle of the x-y plane of the tissue sample. The depth of the source, representing the depth of the tumor in the tissue, was varied from 0 to 6 mm. An ideal detector measuring the Čerenkov photons produced in the tissue was placed adjacent to the top surface of the tissue. A sketch of the geometry can be found in Figure 1(a).

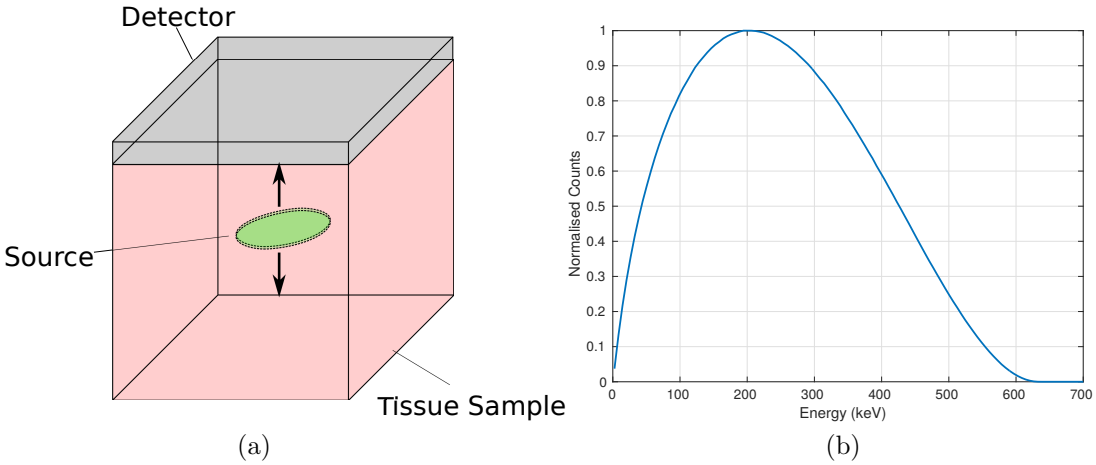

(a) (b)

Figure 1. **(a)**: A sketch of the simulated geometry. The source depth was varied from 0 to 4.0 mm, in 0.25 mm steps, below the top surface of the sample. Additional simulations were performed at 5.0 and 6.0 mm source depth. **(b)**: The simulated energy spectrum of a ^{18}F positron source.

In a separate simulation, the positron energy spectrum of a ^{18}F radioactive source was generated, and a plot of the spectrum can be found in Figure 1(b). In the breast tissue simulation, positrons were created with random energy drawn from the spectrum, and random momentum direction.

Geant4 requires the optical properties of materials to be user-defined. The absorption coefficient of breast tissue was estimated using the model[13]

$$\begin{aligned}\mu_a = {} & BS\mu_{a,\text{oxy}} + B(1-S)\mu_{a,\text{deoxy}} + W\mu_{a,\text{water}} + F\mu_{a,\text{fat}} \\ & + M\mu_{a,\text{melanosome}} + 2.3C_{\text{bili}}\epsilon_{\text{bili}} + 2.3C_{\beta\text{C}}\epsilon_{\beta\text{C}},\end{aligned} \tag{4}$$

where B is the average blood volume fraction, S is the HGb oxygen saturation of mixed arterio-venous vasculature, W is the water content, F is the fat content, M is the melanosome volume fraction, C_{bili} is the bilirubin concentration, and $C_{\beta\text{C}}$ is the β-carotene concentration of the tissue. The absorption spectra of each component is denoted $\mu_{a,\text{x}}$, and the extinction coefficients of bilirubin and β-carotene are given by ϵ_{bili} and $\epsilon_{\beta\text{C}}$, respectively. The coefficients were provided by a number of references, given in Table 1 (all undefined values were set to 0), and the absorption spectra provided in the OMLC Optical Properties Spectra database were used[14] in the range 400 to 1000 nm. Outside of this range, the optical properties were undefined.

Reference	B	S	W	F
Bevilacqua, *et al.* 2000[15]	1.04%	75.5%	29.2%	51.7%
Jakubowski, *et al.* 2004[16]	0.69%	62.6%	6.0%	74.0%
Spinelli, *et al.* 2004[17]	0.67%	66.4%	14.5%	58.0%
Tromberg, *et al.* 1997[18]	1.02%	67.6%	14.4%	65.6%

Table 1. Breast tissue optical parameters.

The scattering coefficient was modelled using the equation[13]

$$\mu_s(\lambda) = a' \left(f_{\text{Ray}} \left(\frac{\lambda}{500nm} \right)^{-4} + f_{\text{Mie}} \left(\frac{\lambda}{500nm} \right)^{-b_{\text{Mie}}} \right), \tag{5}$$

with values $a' = 31.8\ \text{cm}^{-1}$, $f_{\text{Ray}} = 0$, $f_{\text{Mie}} = 1 - f_{\text{Ray}}$, and $b_{\text{Mie}} = 2.741$.[19] The refractive index of the tissue was set to 1.4877 at all wavelengths,[13,15] and the refractive index of the detector was set to the same value, to replicate an ideal detector.

The wavelength of any Čerenkov photon that entered the detector volume was recorded, provided that photon was generated from an interaction within the tissue sample. When the source was placed close to the surface of the tissue, it was possible for positrons to escape the volume and generate photons within the detector. These photons were ignored. The output of each simulation was a wavelength histogram with 1 nm wide bins, and the histograms generated at source depth of 0.5 and 1.0 mm have been plotted in Figure 2(a), and the spectra for the 4 tissue samples with a source depth of 1.0 mm have been plotted in Figure 2(b). Significant differences in the recorded spectra are visible in Figure 2(b), in particular the Spinelli parameters resulted in the highest counts below 600 nm, and the Jakubowski parameters returned high counts between 500 and 600 nm. Each simulation was performed for 500,000 positrons.

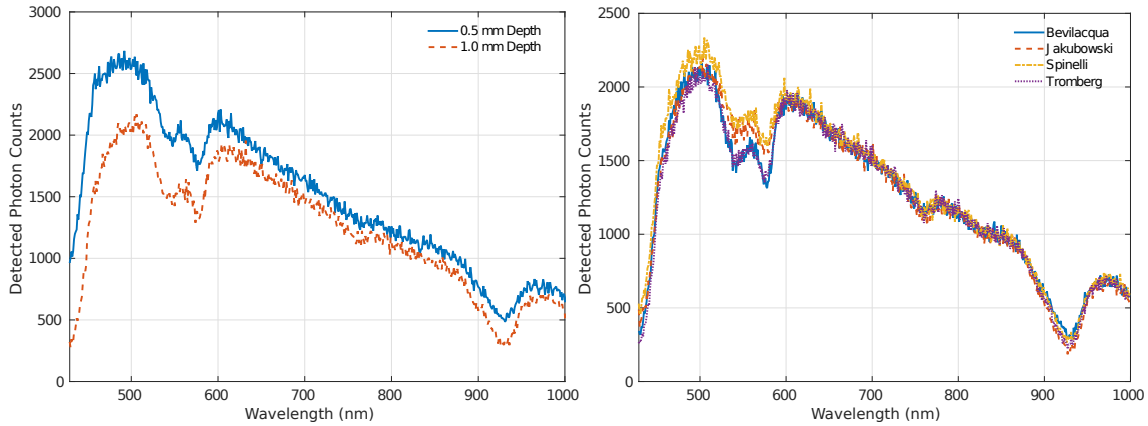

(a) (b)

Figure 2. **(a)**: The detected Čerenkov spectra at a source depth of 0.5 mm (blue, solid line), and 1.0 mm (red, dashed line) using the Bevilacqua parameters.**(b)**: A comparison of the detected spectra at 1.0 mm depth using the Bevilacqua (blue, solid line), Jakubowski (red, dashed line), Spinelli (yellow, dash-dot line), and Tromberg (purple, dotted line) tissue parameters.

4. DEPTH ESTIMATION RESULTS

The MC generated spectra at different depths were used to generate a forward model of the estimated source distribution in a sample, using a low-pass filter at 550 nm and a full-band pass filter. Measurements were simulated at each depth, using the two filters, and the Moore-Penrose pseudoinverse was used to invert the forward model and estimate the source distribution in these simulated measurements. The model was generated using the full-range of cutoff wavelengths for the low-pass filter and it was found that 550 nm minimised the condition number of the forward model, and hence this value was used to generate the results given here. The results, using a single set of parameters for the forward model, for source depths of 0 to 4 mm have been plotted in Figure 3. When the source is close to the surface, some of the positrons escape the tissue without generating Čerenkov photons. Due to these losses, the 0 mm source depth does not have the highest source density at 0mm reconstructed source depth in the figure.

From these results we show that we can distinguish between a source that is less than 1.0 mm from the surface and a source that is 1.0 mm or deeper in the sample.

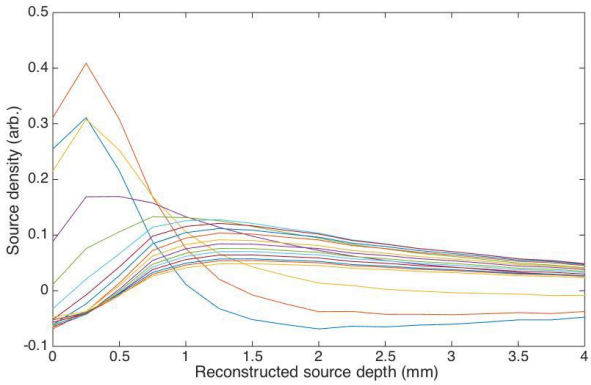

Figure 3. Each contour shows the reconstructed source distribution as a function of depth. Each contour represents a different true source depth varying from 0 to 4 mm in increments of 0.25 mm going from the top contour to the bottom contour, with the exception of 0 mm source depth which is the contour that has the second-highest source density at reconstructed source depth of 0.

5. TISSUE PARAMETER SENSITIVITY ANALYSIS

At each simulated depth, the ratio of low-pass filtered counts (cutoff wavelength of 550 nm) and the full-band pass counts was calculated and has been plotted in Figure 4 for each set of tissue parameters. These results highlight the difficulty in estimating the source depth without a priori information of the tissue absorption coefficients. For example, if 20% of the counts are measured in the low-pass range, then the depth of the source might range from 2.35 mm (using the Tromberg tissue parameters) to 3.4 mm (using the Spinelli tissue parameters). If sources of noise, such as lens transmission, electronic noise, were to be included, the accuracy of this estimate would be further reduced. The curves diverge with increasing source depth, suggesting less accurate source depth reconstruction at larger depths. While our model only indicates whether a source is $<$ 1mm from the surface, the variation in the spectra has implications for further studies that may want to use more a complex model to investigate source depth using the recorded Čerenkov spectrum.

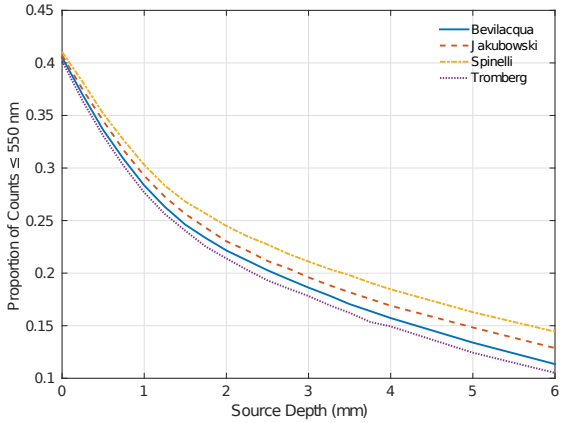

Figure 4. A plot of the ratio of low-pass filtered counts (550 nm) and full-band pass counts for the 4 different sets of tissue parameters (Bevilacqua, blue solid line, Jakubowski, red dashed line, Spinelli, yellow dash-dot line, Tromberg, purple dotted line).

In order to explore the data more fully and investigate whether an accurate depth estimation may be possible when using the entire spectrum of detected optical photons, a Principal Component Analysis (PCA) was performed of the simulated spectra, normalised to the sum. PCA looks for variations and patterns in data sets,

allowing for the reduction of large quantities of data. The first principal component axis gives the largest variation between the data, and the successive components show the largest variation constrained to the orthogonal directions that are remaining. The PCA score values were calculated using MATLAB and have been plotted in Figure 5**(a)**, each depth plotted as a different symbol-colour pair. It is clear from the plot that when the source is close to the surface, the scores from the different tissue values at the same depth are grouped close together. However, as the depth increases the values are no longer clustered together, and hence accurate depth estimation, when the tissue optical parameters are not known is not possible after a depth of approximately 1 mm. Increasing the number of principal components did not appear to improve the performance. A nearest neighbour classifier was applied to the PCA results to estimate source depth of each simulated spectra. The accuracy of the method has been plotted in Figure 5**(b)**. Using the PCA approach it appears that the depth of the source maybe estimated to an accuracy of < 0.5 mm when the source is within 2.5 mm depth of the surface, however this is based on a number of model assumptions that would reduce this accuracy significantly in an experimental setting, for example an ideal lens transmission was assumed. To fully investigate the possibility of estimating the depth using the full spectrum we would need to perform more simulations over a wider range of possible tissue parameters and validate with experimental data.

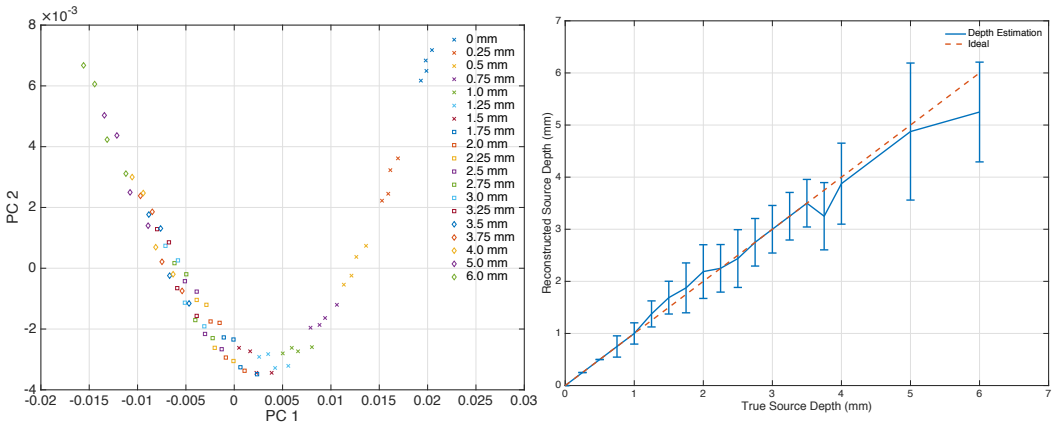

(a) (b)

Figure 5. **(a)**: A scores plot of the first two principal components of the normalised simulated spectra. Each depth has been plotted as a different symbol-colour pair, for the four different tissue parameter sets. **(b)**: The accuracy of the reconstructed source depth method based on the PCA results

6. CONCLUSIONS

We have shown that it is possible to generate limited depth information using CLI, in particular, we can see that we can distinguish between a source that is less than 1.0 mm from the surface and a source that is 1.0 mm or deeper in the sample, when we use a simple low-pass filter approach, an approach that could be realised experimentally by using a lens filter. We also show that small changes in the blood and water proportions in the tissue can affect the depth estimation results significantly, making accurate depth estimation challenging for deeper sources, even when we in the ideal case when we use the entire spectrum.

This work has a number of limitations, and further studies are required to explore this in more detail. The MC model used a simplified geometry, assumed an ideal detector and lens and did not include any noise. The depth estimation models were relatively simplistic and the number of tissue parameters tested was also limited.

ACKNOWLEDGMENTS

This work was funded by Innovate UK project 101674 and EPSRC project EP/N022750/1.

REFERENCES

[1] Houssami, N., Macaskill, P., Marinovich, M. L., and Morrow, M., "The association of surgical margins and local recurrence in women with early-stage invasive breast cancer treated with breast-conserving therapy: A meta-analysis," *Annals of Surgical Oncology* **21**(3) (2014). [doi:10.1245/s10434-014-3480-5].

[2] Houssami, N., Macaskill, P., Marinovich, M. L., Dixon, J. M., Irwig, L., Brennan, M. E., and Solin, L. J., "Meta-analysis of the impact of surgical margins on local recurrence in women with early-stage invasive breast cancer treated with breast-conserving therapy," *European Journal of Cancer* **18**(46) (2010). [doi:10.1016/j.ejca.2010.07.043].

[3] Boughey, J. C., Hieken, T. J., Jakub, J. W., Degnim, A. C., Grant, C. S., Farley, D. R., Thomsen, K. M., Osborn, J. B., Keeney, G. L., and Habermann, E. B., "Impact of analysis of frozen-section margin on reoperation rates in women undergoing lumpectomy for breast cancer: Evaluation of the national surgical quality improvement program data," *Surgery* **156**(1) (2014). [doi:10.1016/j.surg.2014.03.025].

[4] Liu, H., Carpenter, C. M., Jiang, H., Pratx, G., Sun, C., Buchin, M. P., Gambhir, S. S., Xing, L., and Cheng, Z., "Intraoperative imaging of tumors using cerenkov luminescence endoscopy: A feasibility experimental study," *Journal of Nuclear Medicine* **53**(10), 1579–1584 (2012). [doi:10.2967/jnumed.111.098541].

[5] Das, S., Thorek, D. L., and Grimm, J., "Čerenkov imaging," *Advances in Cancer Research* **124**, 213–234 (2014). [doi:10.1016/B978-0-12-411638-2.00006-9].

[6] Grootendorst, M. R., Cariati, M., Pinder, S., Kothari, A., Douek, M., Kovacs, T., Hamed, H., Pawa, A., Nimmo, F., Owen, J., Ramalingam, V., Sethi, S., Mistry, S., Vyas, K., Tuch, D., Britten, A., Van Hemelrijck, M., Cook, G., Sibley-Allen, C., Allen, S., and Purushotham, A., "Intraoperative assessment of tumor resection margins in breast-conserving surgery using 18f-fdg cerenkov luminescence imaging a first-in-human feasibility study," *Journal of Nuclear Medicine* (2016). [10.2967/jnumed.116.181032].

[7] Thorek, D. L. J., Robertson, R., Bacchus, W. A., Hahn, J., Rothberg, J., Beattie, B. J., and Grimm, J., "Čerenkov imaging - a new modality for molecular imaging," *American Journal of Nuclear Medicine and Molecular Imaging* **2**(2), 163–173 (2012). [PMCID:PMC3477724].

[8] Smith, F. A., [*A Primer in Applied Radiation Physics*], World Publishing Co. Pte. Ltd, Singapore (2000).

[9] Frank, I. and Tamm, I., "Coherent visible radiation of fast electrons passing through matter," *Proceedings of the USSR Academy of Sciences* **14**, 109–114.

[10] Grootendorst, M. R., Cariati, M., Kothari, A., Tuch, D. S., and Purushotham, A., "Čerenkov luminescence imaging (cli) for image-guided cancer surgery," *Clinical and translational imaging* , 1–14. [doi:10.1007/s40336-016-0183-x].

[11] Boschi, F. and Spinelli, A. E., "Čerenkov luminescence imaging at a glance," *Current Molecular Imaging* **3**(2), 106–117 (2014). [doi:10.2174/2211555203666141128002406].

[12] S. Agostinelli, et al., "Geant4—A Simulation Toolkit," *Nuclear Instruments and Methods in Physics Research A* **506**(3), 250–303 (2003). [doi:10.1016/s0168-9002(03)01368-8].

[13] Jacques, S. L., "Optical properties of biological tissues: A review," *Physics in Medicine and Biology* **58**(11), R37–R61 (2013). [doi:10.1088/0031-9155/58/11/R37].

[14] Oregon Medical Laser Center, "Optical properties spectra. [online]." Available at: http://omlc.org/spectra/index.html [Accessed 12 Jan. 2016].

[15] Bevilacqua, F., Berger, A. J., Cerussi, A. E., Jakubowski, D., and Tromberg, B. J., "Broadband absorption spectroscopy in turbid media by combined frequency-domain and steady-state methods," *Applied Optics* **39**(34), 6498 (2000). [doi:10.1364/ao.39.006498].

[16] Jakubowski, D. B., Cerussi, A. E., Bevilacqua, F., Shah, N., Hsiang, D., Butler, J., and Tromberg, B. J., "Monitoring neoadjuvant chemotherapy in breast cancer using quantitative diffuse optical spectroscopy: a case study," *Journal of Biomedical Optics* **9**(1), 230 (2004). [doi:10.1117/1.1629681].

[17] Spinelli, L., Torricelli, A., Pifferi, A., Taroni, P., Danesini, G. M., and Cubeddu, R., "Bulk optical properties and tissue components in the female breast from multiwavelength time-resolved optical mammography," *Journal of Biomedical Optics* **9**(6), 1137 (2004). [doi:10.1117/1.1803546].

[18] Tromberg, B. J., Coquoz, O., Fishkin, J. B., Pham, T., Anderson, E. R., Butler, J., Cahn, M., Gross, J. D., Venugopalan, V., and Pham, D., "Non-invasive measurements of breast tissue optical properties using frequency-domain photon migration," *Philosophical Transactions of the Royal Society B: Biological Sciences* **352**(1354), 661–668 (1997). [doi:10.1098/rstb.1997.0047].

[19] Sandell, J. L. and Zhu, T. C., "A review of in-vivo optical properties of human tissues and its impact on PDT," *Journal of Biophotonics* **4**(11-12), 773–787 (2011). [doi:10.1002/jbio.201100062].